RESEARCH ARTICLE OPEN ACCESS

A Machine learning approach in photoacoustic data

Durga Prasad Pragallapati
Dot Net, Team Leader, Jnet technologies pvt ltd, Hyderabad-India

ABSTRACT
A convolutional neural organization was prepared to recognize the area of individual point focuses from pre-beamformed information reenacted with k-Wave to contain different medium sound velocities (1440-1640 m/s), target areas (5-25 mm), and safeguard sizes (1-5 mm). In light of 2,412 haphazardly chose test pictures, the mean hub and parallel point area blunders were 0.28 mm and 0.37 mm, separately, which seem like the standard imaging framework goal for our prepared organization. This ready organization effectively distinguished the two-point area focuses on a solitary picture with mean pivotal and parallel mistakes of 2.6 mm and 2.1 mm, separately. A similar prepared organization indicated the relic area with mean pivotal and parallel errors of 2.1 mm and 3.0 mm, individually. These outcomes exhibit a dependable guarantee to distinguish point focuses without requiring conventional math-based beamforming, prompting the possible end of reflection curios from interventional pictures.
Keywords; - Artificial intelligence, Machine learning

I. INTRODUCTION

Photoacoustic picture quality is profoundly subject to the nature of the beamforming cycle. Generally, beamformers have regarded acoustic wave proliferation as a calculation-based, season-flight estimation representing a signal season of appearance differences. Nonetheless, these season-of-flight estimations don't think that someone can mirror signs on different occasions. The ultrasound transducer will estimate every acoustic reflection, accordingly planning reverberant signals to some unacceptable area.

However, these methodologies depend on similar calculation-based, season-of-flight estimations as those of recorded beamformers, what's more, accordingly likewise fall flat in the presence of solid antiquities brought about by splendid, hyperechoic reflectors. A technique named photoacoustic-guided centered ultrasound (PAFUSion)7 was as of late created to address this challenge by utilizing ultrasound information to mirror the wavefields created by photoacoustic sources and along these lines distinguish reflection antiques for expulsion. This strategy relies upon the suspicion of indistinguishable acoustic gathering pathways for an ultrasound and photoacoustic information, which isn't in every case valid. Engendering and the related season of-flight include tissue properties (for instance, sound speed, weakening, assimilation), tissue type (for example, fat, bone, muscle), tissue thickness, and refraction.

For instance, although CNNs have lately come to fulfillment, neural organizations go back much further, and Nikoonahad et al.11 utilized neural organizations to eliminate ancient rarities in ultrasound pictures by assessing defer capacities dependent on season of-flight data. While this approach targets antiques brought about by sound speed assessment mistakes, it doesn't address the seriously dangerous ancient rarities brought about by acoustic reflections.

This methodology depends on the perception that signals from point sources situated at a similar profundity, for the most part, have comparative wavefront shapes, paying little mind to the medium encompassing properties. The initial move toward utilizing A.I. to eliminate reflection ancient rarities is to precisely recognize these point source areas. Toward this end, we prepared a CNN to distinguish point source areas using mimicked information. At that point, we applied the prepared organization to a free arrangement of reproduced information containing point sources and reflection ancient rarities. We tried our ready

CNN with genuine trial information. The following point source areas may either be shown independently or overlaid on co-enrolled ultrasound, C.T., as well as MRI pictures, which are traditional imaging modalities for picture guided mediations and careful route.

II. METHODS

We prepared our CNN utilizing reproduced photoacoustic channel information and the broadly accessible AlexNet network architecture.8 The photoacoustic channel information was made with k-Wave simulations12, 13 and viewed as an information picture. These pictures were haphazardly part of preparing (80%), approval (10%), and test (10%) sets. The yield of the calculation contained the point target 2D area in pictures made under the conditions, as shown in Fig. 1. The means to accomplish the 2D point area included nonlinearity with amended straight units, max pooling, and relapse with L2 standardization

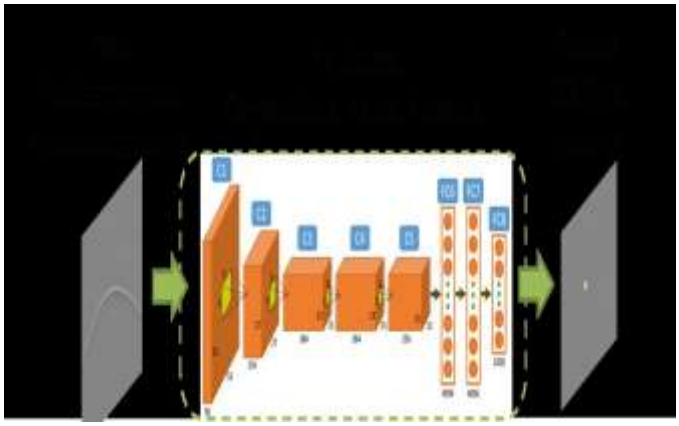

Figure 1: A convolutional neural network was trained to relate pre-beamformed acoustic data to point source locations.

III. RESULTS & DISCUSSION

A. One Simulated Source

The aftereffects of 2,412 test set pictures uncovered that the usual point area blunder was 0.18 mm and 0.27 mm in the hub and sidelong measurements, separately. The mean blunders commonly diminished as a hub and parallel distance expanded, as outlined with the crate hair plots of Fig. 2. The top and lower part of each case speaks to the 75th and 25th percentiles of the estimations separately. The line inside each crate speaks to the middle estimation, and the bristles (i.e., lines stretching out above and underneath each crate) speak to the reach.

The blunders detailed in Fig. 2 can be viewed as our imaging framework's goal when the known variety in sound speed goes from 1440-1640 m/s and the known variety in objective size goes from 1-5 mm. With the conventional beamforming suspicion of a fixed 1540 m/s sound speed, a medium known to comprise sound speeds inside ±100 m/s of the expected sound speed would make the traditional pictures have sound speed blunders to greatest distance mistakes of 6.5%.

These outcomes recommend that the proposed calculation distinguish focuses on the messiness, and different ancient rarities brought about by speed of sound mistakes from numerous tissue layers.

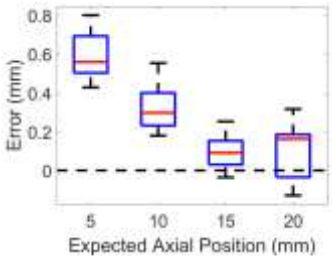

(a)

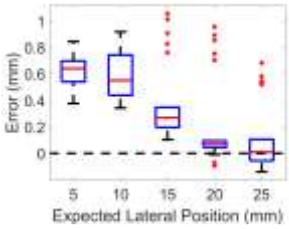

(b)

Figure 2: Summary of point location errors obtained with the trained CNN in the (a) axial and (b) lateral dimensions of the image.

B. Two SimulatedSources

To explore the achievability of identifying more than one point source in a solitary picture, apply CNN to 20 images containing two sign sources. Our prepared CNN effectively distinguished the source areas with mean hub and parallel mistakes of 2.6 mm and 2.1 mm, separately. To accomplish this recognition, we saw that the organization was one-sided toward identifying the right-most wavefield.

A genuine sign and a relating reflection antique were then reenacted in 20 pictures, as exhibited in

Fig. 3 (base). Even though they show up at a similar profundity, which shows that one of these wavefronts starts from an antique. Although our prepared CNN recognized the areas of both the sources and the ancient reflection rarities with comparative precision, it couldn't differentiate genuine signs from antiquities since it was not yet prepared to identify these differences. However, this is the ultimate objective of the proposed method.

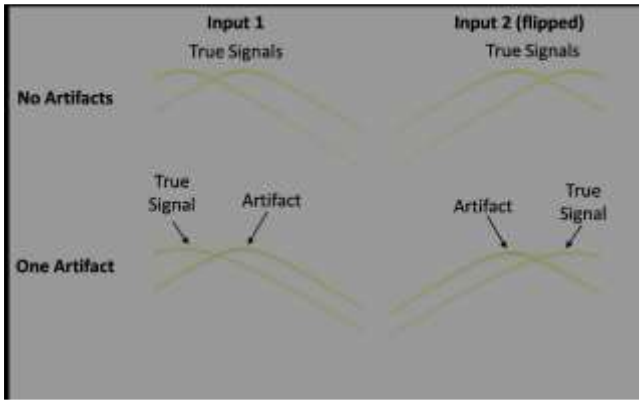

Figure 3: Examples of two-point sources in a single image.

C. Artifact Detection

One possible way to differentiate relics from genuine signs is to take care of these two wavefields' recognized areas as contributions to an autonomous k-Wave reproduction. At that point, contrast the subsequent wavefields with those of the first picture. This methodology is sensible because antiquities will, in general, show as clearly different wavefield shapes from genuine signs when they show up at a wrong profundity. One alternative to make this qualification is to break down the waves' state at the pinnacle area and build histograms of the wavefield crude information (for example, the picture y-organizes). Since our CNN is prepared to foresee both genuine signs and curios' wavefield areas, we can sensibly prepare a classifier to recognize these two cases.

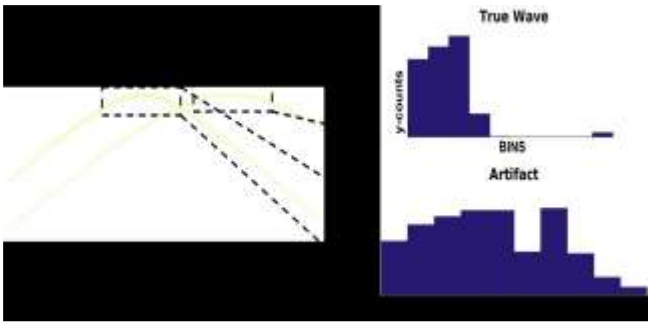

Figure 4: Demonstration of a histogram-based wavefield shape matching technique. The histogram shows the axial location of the wavefield segments in the dashed boxes. Note the differences when comparing the accurate wave histogram (top) to that of the artifact (bottom).

D. Application to Experimental Data

To show that our methodology has expansive pertinence to numerous kinds of information, we tried our prepared CNN on exploratory details, which has differing qualities when contrasted with reenacted information. The noisier foundation, the inadequate wavefield curve, and the nonuniform sign powers over the wavefield in Fig. 5 show the crude channel information from a 3-mm measurement pole lowered in the water.14 The hub and sidelong places of the bar regarding the left corner of the ultrasound test (which compares to the upper left corner of the photoacoustic picture) was 6 mm and 11 mm, separately. Our prepared CNN assessed these situations inside ⇠2 mm in each measurement, distinguishing the point source areas as 4.21 mm (hub) and 13.01 mm (parallel).

Figure 5: Experimental data from a 3 mm diameter blood vessel phantom.

The blunder is more significant than that gotten with the single-source results (Fig. 2), likely because of the wavefield's favoritism, which has a similar appearance aside from the full wavefield saw when two wavefields cover (Fig. 3). Albeit may need extra preparation with fractional wavefields to decrease the mistake. This outcome features the potential for our way to deal with be prepared with reproduced information, at that point executed to distinguish point areas in trial information.

IV. CONCLUSIONS

This work speaks to the principal showing of A.I. applied to photoacoustic information representation. We prepared a CNN utilizing mimicked boundaries (for example, 2D point target positions, medium sound speeds, and target radii) to anticipate reasonable picture development boundaries straightforwardly from crude, pre-beamformed information. Our starter results show the achievability of the proposed approach. Future work will test elective CNNs to recognize numerous point sources, halfway wavefields, and distinguish curios for expulsion.

REFERENCES

[1] Muyinatu A Lediju Bell, Nathanael P Kuo, Danny Y Song, Jin U Kang, and Emad M Boctor. In vivo
visualization of prostate brachytherapy seeds with photoacoustic imaging. Journal of Biomedical Optics,
19(12):126011–126011, 2014.
[2] Muyinatu A Lediju Bell, Xiaoyu Guo, Danny Y Song, and Emad M Boctor. Transurethral light delivery
for prostate photoacoustic imaging. Journal of Biomedical Optics, 20(3):036002–036002, 2015.
[3] Muyinatu A Lediju Bell, Anastasia K Ostrowski, Ke Li, Peter Kazanzides, and Emad M Boctor. Localization
of transcranial targets for photoacoustic-guided endonasal surgeries. Photoacoustics, 3(2):78–87, 2015.
[4] Gadde, S. S. (2020). Artificial Intelligence - The Future of Radiology. International Journal for Research in Applied Science and Engineering Technology. 8. 10.22214/ijraset.2020.6043.
[5] Emma R Hill, Wenfeng Xia, Matthew J Clarkson, and Adrien E Desjardins. Identification and removal of
laser-induced noise in photoacoustic imaging using singular value decomposition. Biomedical Optics Express,
8(1):68–77, 2017.
[6] Muyinatu A Lediju Bell, Nathanael Kuo, Danny Y Song, and Emad M Boctor. Short-lag spatial coherence
beamforming of photoacoustic images for enhanced visualization of prostate brachytherapy seeds. Biomedical
Optics Express, 4(10):1964–1977, 2013.
[7] Gadde, S. S., & Kalli, V. D. R. Applications of Artificial Intelligence in Medical Devices and Healthcare. 10.33144/23478578/IJCST-V8I2P27
[8] Alex Krizhevsky, Ilya Sutskever, and Geoffrey E Hinton. Imagenet classification with deep convolutional
neural networks. In Advances in neural information processing systems, pages 1097–1105, 2012.
[9] Gadde, S. S., & Kalli, V. D. R. (2020). Technology Engineering for Medical Devices-A Lean Manufacturing Plant Viewpoint. 10.17148/IJARCCE.2020.9401
[10] David Eigen, Christian Puhrsch, and Rob Fergus. Depth map prediction from a single image using a
multi-scale deep network. In arXiv:1406.2283 [cs.CV], 2014.
[11] M Nikoonahad and DC Liu. Medical ultrasound imaging using neural networks. Electronics Letters,
26(8):545–546, 1990.
[12] Bradley E Treeby and Benjamin T Cox. k-Wave: MATLAB toolbox for the simulation and reconstruction
of photoacoustic wave fields. Journal of Biomedical Optics, 15(2):021314–021314, 2010.
[13] Gadde, S. S., & Kalli, V. D. R. Artificial Intelligence To Detect Heart Rate Variability. 10.33144/23939516/IJETA-V7I3P2

[14] Neeraj Gandhi, Sungmin Kim, Peter Kazanzides, and Muyinatu A. Lediju Bell. Accuracy of a novel photoacoustic-based approach to surgical guidance performed with and without a da Vinci robot. SPIE BiOS, 2017.
[15] Gadde, S. S., & Kalli, V. D. R. Descriptive Analysis of Machine Learning and Its Application in Healthcare. 10.33144/23478578/IJCST-V8I2P28
[16] Gadde, S. S., & Kalli, V. D. R. Medical Device Qualification Use. 10.17148/IJARCCE.2020.9410